

AD-A133 460

THE NATURE OF QUASICLEAVAGE FRACTURE IN TEMPERED 55 NI  
STEEL AFTER HYDROG. (U) CALIFORNIA UNIV BERKELEY DEPT  
OF MATERIALS SCIENCE AND MINERA. Y H KIM ET AL.

1/1

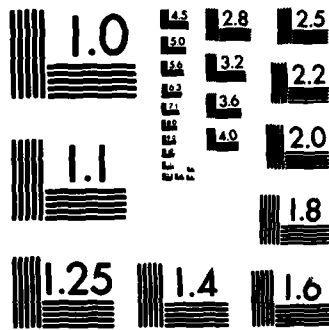
UNCLASSIFIED

OCT 82 TR-12 N00014-75-C-0154

F/G 11/6

NL





MICROCOPY RESOLUTION TEST CHART  
NATIONAL BUREAU OF STANDARDS-1963-A

13

AD-A133460

THE NATURE OF QUASICLEAVAGE FRACTURE  
IN TEMPERED 5.5 Ni STEEL  
AFTER HYDROGEN CHARGING

by

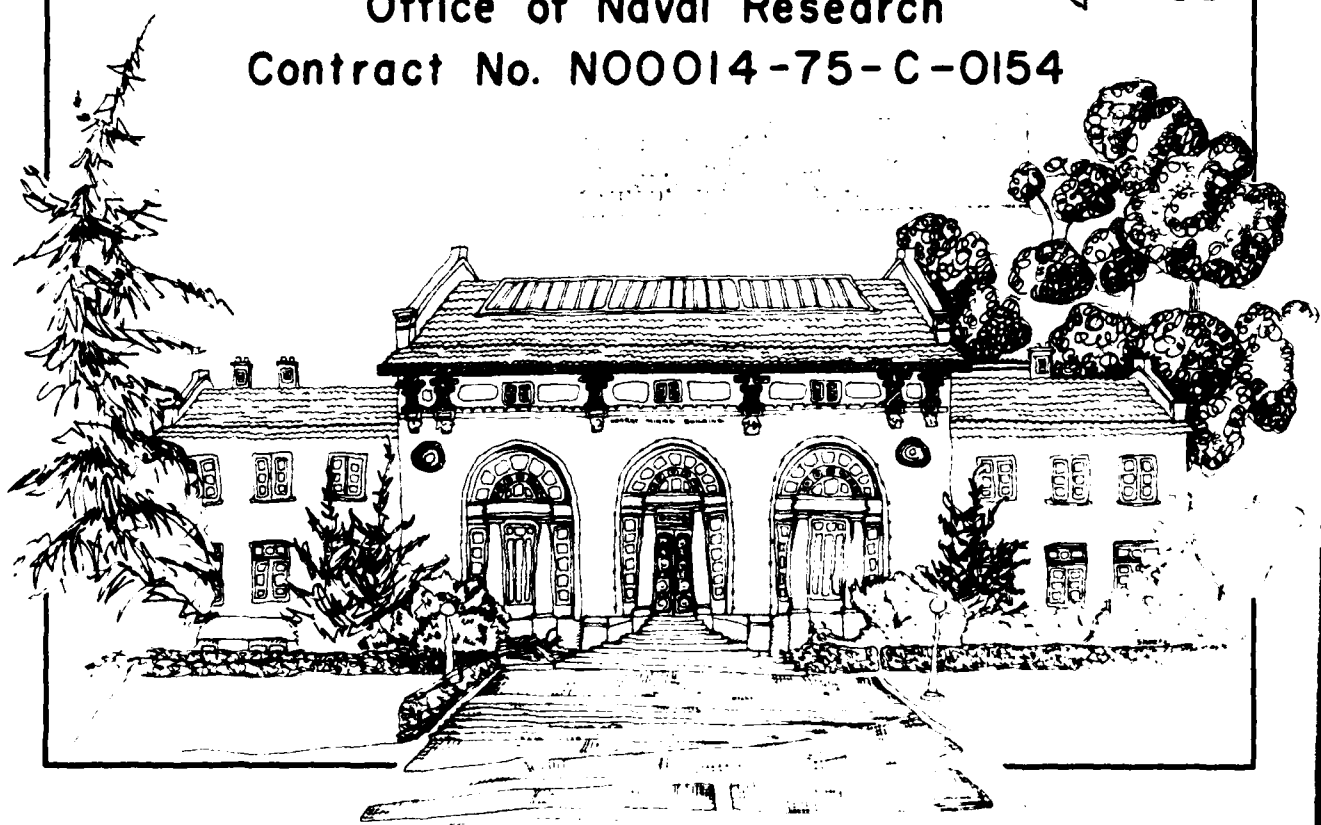
Y. H. Kim and J.W. Morris, Jr.

Department of Materials Science and Engineering  
University of California, Berkeley

October, 1982

Technical Report No. 12  
Office of Naval Research  
Contract No. N00014-75-C-0154

DTIC  
SELECTED  
OCT 12 1983  
A



DTIC FILE COPY

83 09 30 019

REPORT DOCUMENTATION PAGE		READ INSTRUCTIONS BEFORE COMPLETING FORM
1. REPORT NUMBER #12	2. GOVT ACCESSION NO. AD-A133460	3. RECIPIENT'S CATALOG NUMBER
4. TITLE (and Subtitle) THE NATURE OF QUASICLEAVAGE FRACTURE IN TEMPERED 5.5NI STEEL AFTER HYDROGEN CHARGING		5. TYPE OF REPORT & PERIOD COVERED
		6. PERFORMING ORG. REPORT NUMBER
7. AUTHOR(s) Y. H. Kim and J. W. Morris, Jr.		8. CONTRACT OR GRANT NUMBER(s) N00014-75-C-0154
9. PERFORMING ORGANIZATION NAME AND ADDRESS University of California Dept. of Materials Science & Mineral Engineering Berkeley, CA 94720		10. PROGRAM ELEMENT, PROJECT, TASK AREA & WORK UNIT NUMBERS NR 031-762
11. CONTROLLING OFFICE NAME AND ADDRESS NAVAL SEA SYSTEMS COMMAND Washington, D.C. 20362		12. REPORT DATE October, 1982
		13. NUMBER OF PAGES 24
14. MONITORING AGENCY NAME & ADDRESS (if different from Controlling Office) OFFICE OF NAVAL RESEARCH 800 N. Quincy Street Arlington, VA 22217		15. SECURITY CLASS. (of this report) Unclassified
		15a. DECLASSIFICATION/DOWNGRADING SCHEDULE
16. DISTRIBUTION STATEMENT (of this Report)		
17. DISTRIBUTION STATEMENT (of the abstract entered in Block 20, if different from Report)		
18. SUPPLEMENTARY NOTES Submitted to Metallurgical Transactions.		
19. KEY WORDS (Continue on reverse side if necessary and identify by block number) Hydrogen embrittlement, steels, lath martensite, fracture, quasicleavage, interlath fracture.		
20. ABSTRACT (Continue on reverse side if necessary and identify by block number) Quenched and tempered 5.5Ni steel was embrittled by hydrogen charging and broken in air at room temperature. The primary fracture mode was transgranular quasicleavage. The quasicleavage facets were studied by scanning electron fractography and by transmission electron microscopy of profile fractographic specimens. The latter were prepared by plating the fracture surface with nickel and thinning so that the fracture surface was contained within the region of the specimen that was transparent to the electron beam. The (cont.)		

THE NATURE OF QUASICLEAVAGE FRACTURE IN TEMPERED 5.5NI STEEL  
AFTER HYDROGEN CHARGING

Abstract cont.

fracture surface generally followed martensite lath boundaries. In addition, interlath microcracks were frequently found in the material immediately beneath the fracture surface. These results suggest that transgranular hydrogen embrittlement in this steel is primarily an interlath cracking phenomenon. Since the lath boundary planes tend to lie in  $\{110\}$ , the results also explain the prevalence of  $\{110\}$  quasicleavage in the embrittled specimens, which contrasts with the  $\{100\}$  cleavage found in uncharged specimens broken below the ductile-to-brittle transition temperature.



## I. Introduction

When high strength martensitic steels are embrittled by hydrogen they may fail either by intergranular separation along the prior austenite grain boundaries or by transgranular fracture along planes which traverse the prior austenite grains. The transgranular failure mode superficially resembles the transgranular cleavage fracture found in similar steels when they are broken below their ductile-to-brittle transition temperatures. Recent research has shown, however, that there are significant differences. The most striking of these is the fracture plane itself, which is predominantly  $\{100\}$  in low-temperature fracture, but is often found to be  $\{110\}$  or  $\{112\}$  after hydrogen embrittlement [1-4]. While the  $\{100\}$  plane is the natural cleavage plane in BCC iron, the  $\{110\}$  and  $\{112\}$  are the dominant slip planes.

The coincidence between the fracture plane and the dominant slip plane in steels that have been embrittled by hydrogen has led several authors to suggest that embrittlement occurs through a "glide plane decohesion" resembling that occasionally found in the basal plane fracture of hexagonal close-packed metals [1,2,5,6]. The evidence supporting this hypothesis is indirect, however, and there is an alternative explanation for the crystallography of transgranular fracture which is based on the prevalence of  $\{110\}$  and  $\{112\}$  planes in the boundaries of martensite plates and subgrains in high strength steel. The  $\{110\}$  plane is the usual low angle boundary plane separating laths in lath martensitic steels; the  $\{112\}$  plane is the boundary plane when adjacent laths are twin-related [7,8]. Both the  $\{110\}$  and  $\{112\}$  planes are common boundary planes for the subgrains formed in iron after severe deformation or tempering [9]. It is therefore possible that transgranular fracture in embrittled high strength steels follows lath or subgrain boundaries, and hence resembles intergranular fracture more than either transgranular cleavage or glide plane decohesion.

To clarify this issue we carried out high resolution studies of the fracture path in a 5.5Ni steel which had been embrittled by hydrogen charging. 5.5Ni is a high alloy steel that is sold commercially for structural use at cryogenic temperatures. Its microstructure is well known, and typically contains well defined laths of dislocated martensite that are organized into packets (Fig. 1). The laths within a packet are separated by highly dislocated, low angle boundaries that tend to follow {110} planes (Fig. 2) [7]. Below its ductile-to-brittle transition temperature 5.5Ni steel fractures in a brittle transgranular mode along {100} cleavage planes [7,8]. Since the microstructure and mechanical properties of 5.5Ni steel are well known and techniques have been developed for high resolution studies of its transgranular fracture features, this alloy seemed a natural candidate for research on transgranular hydrogen embrittlement.

## II. Experimental Procedure

The research alloy was a commercial 5.5Ni steel provided by the Nippon Steel Corporation. The alloy was supplied as a 35mm plate. Its composition was determined to be: Fe-5.75Ni-0.93Mn-0.5Mo-0.16Cr-0.06C-0.006P-0.005S. The alloy was annealed at 1200C for two hours to remove the effects of prior treatment, and then given a quench and temper treatment to eliminate any tendency toward fracture along the prior austenite grain boundaries. It was austenitized at 800C for one hour, water quenched, and tempered at 600C for one hour. Standard sized charpy impact specimens were cut from the tempered plate, fatigue precracked, and fractured slowly in three-point bending.

The hydrogen charged specimens were made by cathodic charging in 1N H<sub>2</sub>SO<sub>4</sub> using a platinum sheet anode. Small amounts of As<sub>2</sub>O<sub>3</sub> and CS<sub>2</sub> were added to the electrolyte to prevent recombination of hydrogen gas [3]. The specimens were precharged for 24

hours at a current density of 100 milliamps per square centimeter. They were fractured at room temperature in air as soon as possible after completion of the charging.

Fractographic analyses of the broken specimens included optical and scanning electron microscopy to determine the fracture mode, chemical etching to identify the quasicleavage plane [1], and transmission electron microscopy on "profile fractographic" [10,11] specimens to observe the fracture plane and the associated subsurface damage. The chemical etching was done using the three step procedure and the reagent suggested by Matsuda, et al. [12]. The profile fractographic specimens were prepared by electroplating the fracture surface with nickel and then slicing the specimen along the direction of crack propagation and perpendicular to the fracture surface. After mechanical polishing to reduce thickness, thin foil specimens were prepared by a combination of electropolishing and ion beam milling [13]. A number of foils were obtained which contained the profile of the fracture surface within the region that was transparent to 100kV electrons. The foils were then examined in a transmission electron microscope at an operating voltage of 100kV.

### III. Results

#### A. Microstructure

The microstructure of the tempered specimens is illustrated in Figures 1 and 2. The microstructure consists of packets of dislocated martensite laths. The laths within a packet are usually separated by highly dislocated low angle boundaries which lie nearly parallel to {110} planes (Fig. 2). Twin boundaries along {112} planes and high angle boundaries are also occasionally found. As a consequence of tempering, the dislocations within the laths are partially polygonized into subgrains. The tempering temperature, 600C, is slightly within the intercritical range.

There is hence some retained austenite in the microstructure, approximately 2 per cent by volume, and there are occasional fresh martensite laths which are due to the retransformation of austenite formed during tempering.

### B. Mechanical Test Results

Figure 3 shows typical load-deflection curves for 3-point bending specimens fractured with and without hydrogen charging. The hydrogen-free specimen had a high value of the fracture toughness, approximately  $330 \text{ MPa}\cdot\text{m}^{1/2}$  ( $300 \text{ ksi}\cdot\text{in}^{1/2}$ ), and fractured in a totally ductile manner as illustrated by the scanning electron fractographs presented in Figure 4. Hydrogen charging caused a drop in the load-deflection curve and a substantial decrease in the fracture toughness to approximately  $180 \text{ MPa}\cdot\text{m}^{1/2}$  ( $160 \text{ ksi}\cdot\text{in}^{1/2}$ ). In this case, also, the sample was significantly deformed during fracture. The primary fracture mode was quasi-cleavage (Fig. 5), with an occasional admixture of ductile rupture. Secondary quasicleavage cracks were observed branching away from the fracture surface.

### C. Detailed Analysis of Quasicleavage Fracture

A close examination of scanning electron fractographs of the hydrogen-embrittled specimens (for example, Fig. 5) reveals that the quasicleavage portions of the fracture surface are decorated by fine, lath-like features which are comparable in dimension to the martensite laths shown in Figure 2. The etch pits formed on these surfaces (Fig. 6) show the elongated-hexagon shape which is typical of etch pits on  $\{110\}$  surfaces [1,2]. These observations suggest that the fracture propagates preferentially along the martensite laths, and lies either in or parallel to the lath boundaries. Optical and scanning electron micrographs of etched fracture profile specimens (for example, Fig. 7) confirm this conclusion, and suggest that the predominant fracture mode is lath boundary separation.

Transmission electron micrographs of the profile fractographic specimens afford a more detailed view of the fracture surface and the immediate subsurface region. Four example micrographs are presented in Figure 8(a-d). There is some uncertainty in the precise location of the fracture surface since the matching surface is unavailable and since it is possible that the specimen surface was slightly altered by the plating process. It is clear, however, that the fracture surface tends to parallel the long axis of the martensite laths. It also appears that the fracture surface lies in the lath boundaries over almost its whole length. Its probable deviations from the lath boundary, for example, the segments marked with an asterisk at the lower right in Figure 8(d), seem to represent short steps connecting longer segments of interlath fracture. The material immediately beneath the fracture surface sometimes has a simple diffraction pattern, showing that it is a single martensite packet which has not been severely deformed. In this case, which is exemplified by Fig. 8(b,d), the plane of fracture can be identified and is close to  $\{110\}$ . Other subsurface regions yield diffraction patterns in which the spots are spread into arcs along the diffraction circle, as in Figure 8(a). These regions were evidently deformed during fracture.

The high resolution transmission electron fractographs also reveal a dense population of fine secondary cracks immediately beneath the fracture surface. These secondary microcracks are present in all micrographs; they are located by solid arrows in Figure 8. The microcracks are almost certainly associated with the fracture process since they are commonly found in the first few micrometers of material beneath the fracture surface, but are not found in specimens taken from deeper within the fractured sample. The secondary microcracks almost invariably lie in and along lath boundaries. They usually initiate at irregularities in the lath boundary such as boundary intersections, steps, or foreign particles, and continue as sharp flaws in the boundary

plane. In one isolated instance, shown in Fig. 8(c), a microcrack was located in the interior of a lath. This microcrack emanates from an impurity particle which is probably a carbide.

#### IV. Discussion and Conclusion

The results presented above strongly suggest that the quasicleavage fracture associated with hydrogen embrittlement in 5.5Ni steel is predominantly interlath fracture. The evidence supporting this conclusion includes the following. The superficial quasicleavage plane is the common lath boundary plane. All optical, scanning and transmission electron micrographic views of the fracture surface reveal an apparent interlath fracture. Interlath microcracks are common in the material immediately beneath the fracture surface. Translath fracture segments are only occasionally found, and seem to be either internal microcracks due to impurity particles or short steps connecting interlath features. Hydrogen-induced transgranular quasicleavage hence appears to be an interlath phenomenon which phenomenologically resembles intergranular fracture.

The results also suggest a mechanism for hydrogen-induced quasicleavage: interlath microcracks nucleate in the stressed region ahead of the crack tip at irregularities in the lath boundaries, propagate along the boundaries, and eventually link together, sometimes across laths, to form the macroscopic fracture surface. The observations supporting this mechanism include the following. The interlath microcracks near the fracture surface almost certainly form ahead of the propagating crack tip, since the stress required to nucleate them would be relieved once the crack tip had passed. The transmission electron fractographs contain clear evidence for microcrack propagation along lath boundaries. The continuity of the lath boundary network permits the growing microcracks to link together; parallel microcracks may also link by shearing the intervening bulk material. This

mechanism explains both the  $\{110\}$  quasicleavage plane and the microscopic roughness of the quasicleavage fracture surface, which is an expected consequence of the irregularities in both the lath boundary network and the microcrack nucleation process. While the  $\{112\}$  quasicleavage plane was not found in the limited number of micrographs examined in the present work,  $\{112\}$  facets can also arise from interlath fracture since  $\{112\}$  boundaries separating twin-related laths are known to be present in the usual microstructure of the alloy.

The results and conclusions reported here do not deny the common hypothesis that hydrogen embrittlement is related to the formation of hydrogen atmospheres around dislocations [6,14,15]; the lath boundaries are highly dislocated, and hydrogen atmospheres will certainly affect their interfacial cohesion. It is also possible that dislocation glide influences the interlath fracture; the embrittled specimens undergo substantial plastic deformation during fracture and, in some cases, the material immediately adjacent to the quasicleavage fracture surface has been significantly deformed. The results seem to establish, however, that classic "glide plane decohesion" is a minor factor in the hydrogen-induced quasicleavage of 5.5Ni steel if it is relevant at all. Moreover, since the quasicleavage is predominantly interfacial, it is not necessary to assume that hydrogen has any relevant effect on the bonding characteristics of the bulk alloy.

While the results reported here refer to a particular alloy and heat treatment, we suspect that they are widely applicable to high strength martensitic steels. The mechanism of hydrogen embrittlement which we have apparently observed is a plausible mechanism in any martensitic steel. The various scanning electron micrographs published by Kikuta and coworkers [1,2,15] seem to show a predominantly lath boundary mode in the transgranular fracture of embrittled martensitic steels. Moreover, the interlath mode will automatically yield a quasicleavage surface which is both irregular on a microscopic scale and dominated by  $\{110\}$

fracture facets, in agreement with common experimental results from a variety of steels.

A similar process seems to operate in Fe-based alloys which contain no martensite phase. For example, Nagumo and coworkers [9] studied the hydrogen embrittlement of pure iron and found that embrittlement occurred only after the iron had been strained sufficiently to form well-defined subgrains. Fracture then proceeded through the nucleation and linkage of microfractures in the subgrain boundaries. In this case also the dominant mechanism of "transgranular" hydrogen embrittlement is apparently interfacial decohesion along internal boundaries.

#### ACKNOWLEDGMENTS

The authors are grateful to the Nippon Steel Company for supplying the research material and to W. Salesky, Materials and Molecular Research Division, Lawrence Berkeley Laboratory for assistance in the preparation of the profile fractographic specimens. This research was supported by the Office of Naval Research under Contract No. N00014-75-C-0154, NR 031-762.

#### REFERENCES

1. Y.Kikuta, T.Araki and T.Kuroda, Fractography in Failure Analysis, ASTM STP 645, American Society for Testing and Materials, 1978, p. 107
2. Y.Kikuta and T.Araki, Hydrogen Effects in Metals, I.M.Bernstein and A.W.Thompson, eds., TMS-AIME, New York, 1981 p.309

3. F.Nakasoto and I.M.Bernstein, Met. Trans. A, 1978, vol.9A, p.1317
4. I.M.Bernstein, Met. Trans. A, 1970, vol.1, p.3143
5. Y.Takeda and C.J.McMahon,Jr., Met. Trans. A, 1981, vol. 12A, p.1255.
6. C.J.McMahon,Jr., Hydrogen Effects in Metals, I.M.Bernstein and A.W.Thompson, eds., TMS-AIME, New York, 1981, p. 219
7. J.I.Kim, Ph.D Thesis, Department of Materials Science and Mineral Engineering, University of California, Berkeley,1979
8. J.I.Kim, C.K.Syn and J.W.Morris,Jr., Met.Trans.(in press)
9. M.Nagumo, H.Morikawa and K.Miyamoto, Proceedings JIMIS-2, Hydrogen in Metals, Suppl. Trans. Japan Inst. Metals, 1980, vol. 21, p.405
10. H.Haga and H.Mimura, Trans. Japan Inst. Metals, 1972, vol. 13, p.155
11. C.K.Syn, B.Fultz and J.W.Morris,Jr., Met.Trans. A, 1978, vol. 9A, p. 1635
12. S.Matsuda, T.Inoue, H.Mimura and Y.Okamura, Toward Improved Ductility and Toughness, Climax Molybdenum Development Co. (Japan) Ltd., Kyoto, 1972, p.45
13. S.Hogmark, H.Swahn and O.Vingsbo, Ultramicroscopy, 1975, vol.1, p.113
14. J.Tien, S.Nair and R.Jensen, Hydrogen Effects in Metals, I.M.Bernstein and A.W.Thompson, eds., TMS-AIME, New York, 1981, p.37

15. Y.Kikuta, Hydrogen Effects in Metals, I.M.Bernstein and A.W.Thompson, eds., p.755

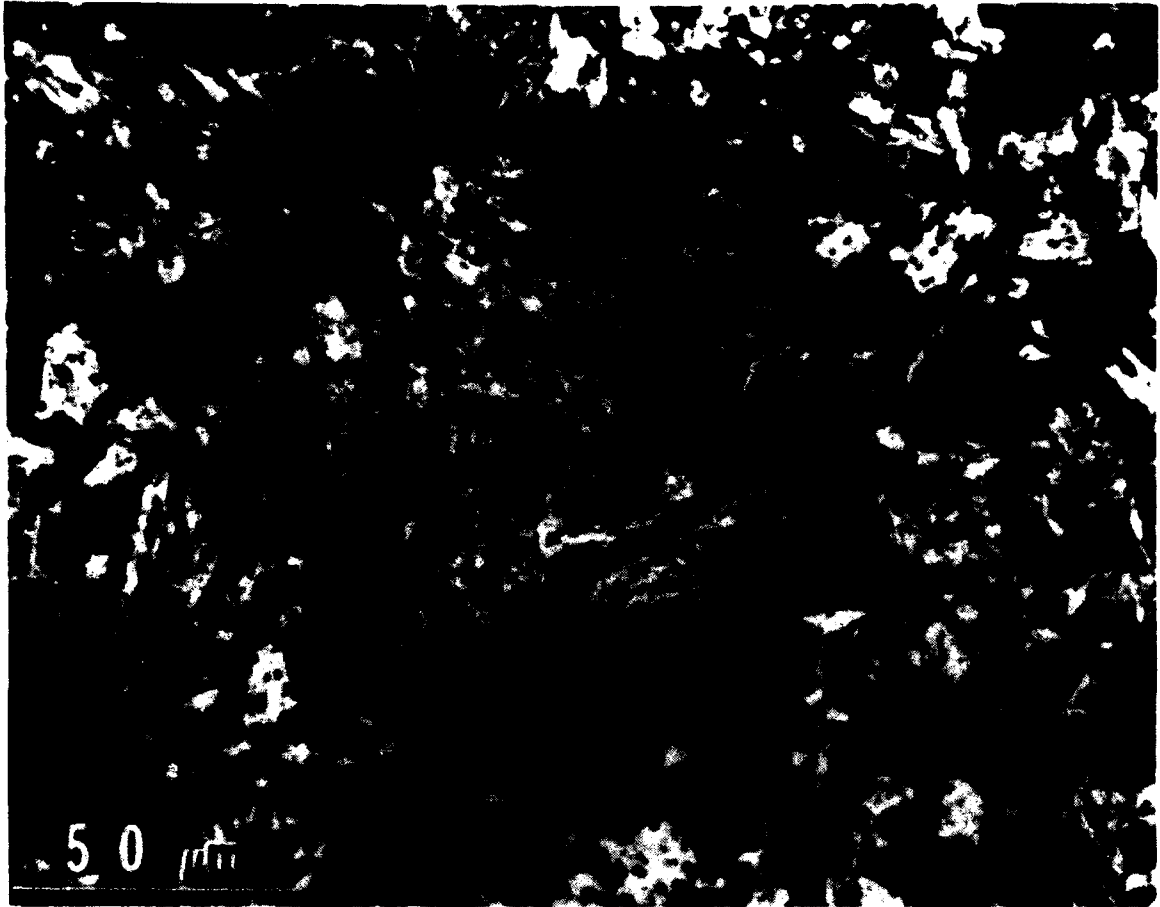


Figure 1. Optical micrograph of quenched and tempered 5.5Ni steel.

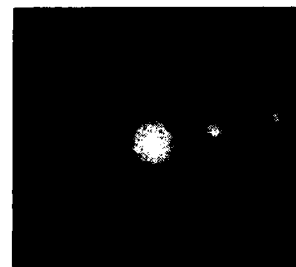
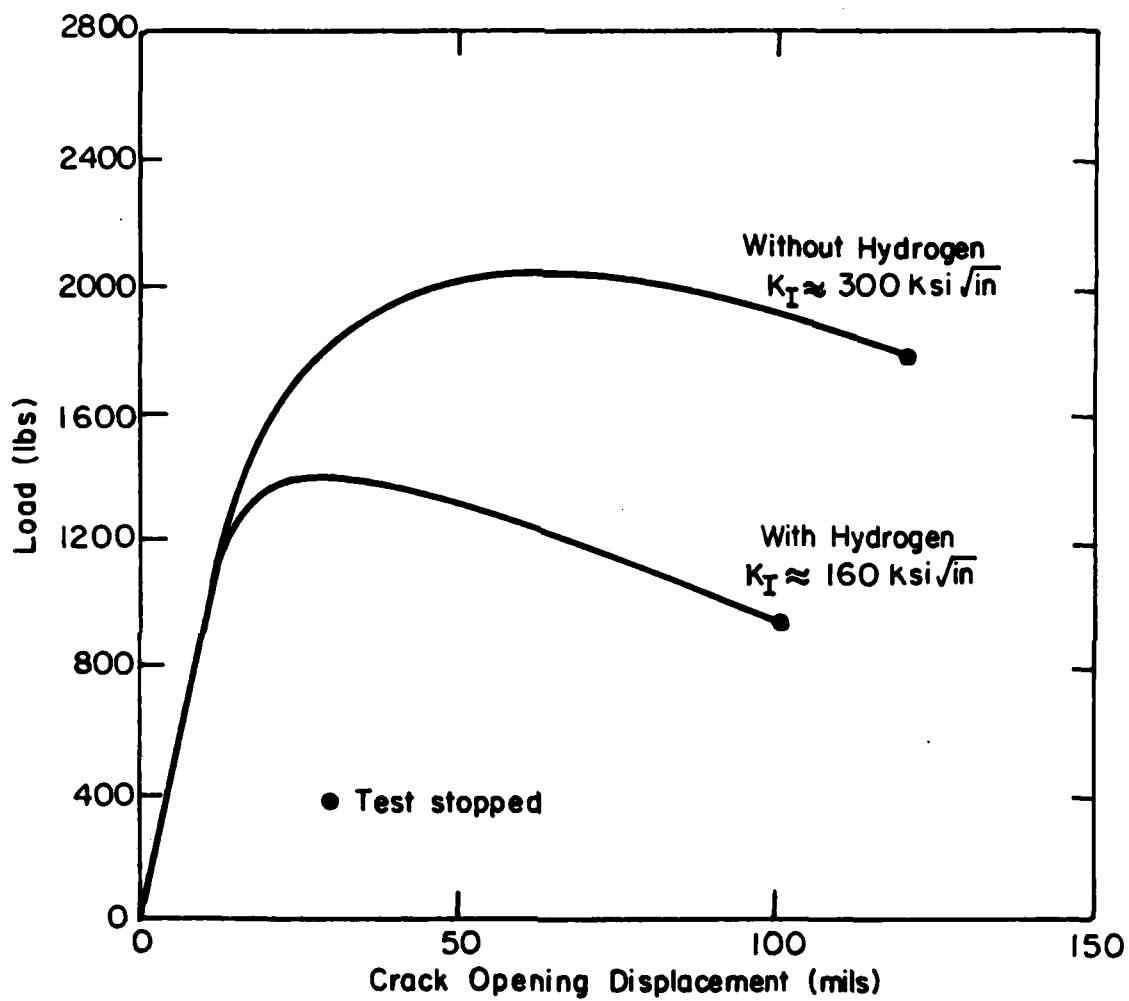


Figure 2. Transmission electron micrograph showing the appearance of martensite laths in tempered 5.5Ni steel.



XBL 829-6512

Figure 3. The load-displacement curves of three-point bend specimens of 5.5Ni steel tested before and after hydrogen charging.

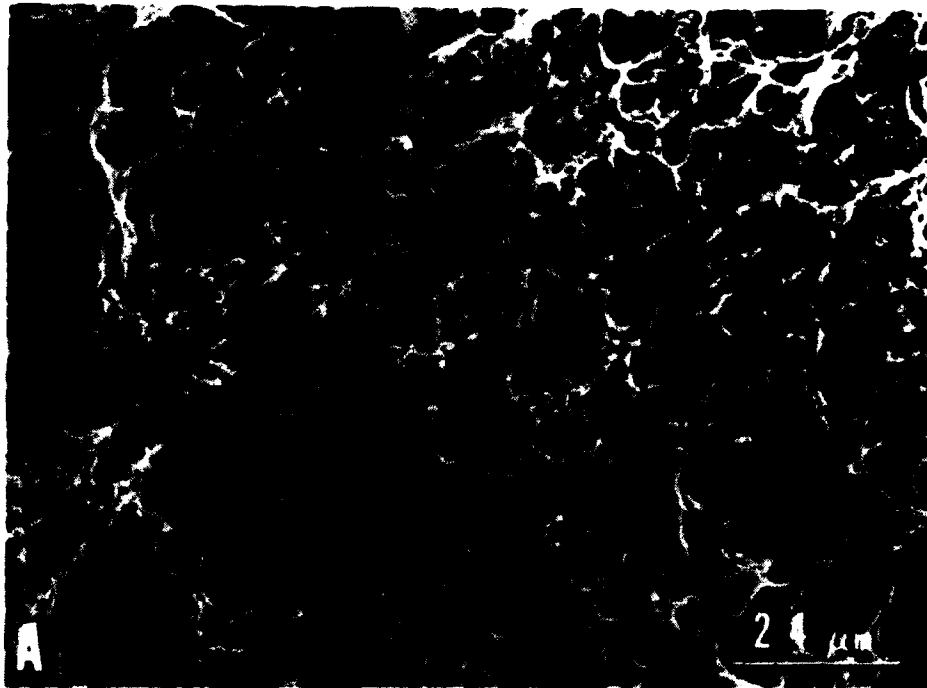


Figure 4. Scanning electron fractographs of a three-point bend specimen broken in the uncharged condition.  
(A) Low magnification fractograph showing the ductile rupture fracture mode.



(B) Higher magnification view of region outlined in A.

(A) Low magnification fractograph showing the presence of quasi-cleavage fracture.

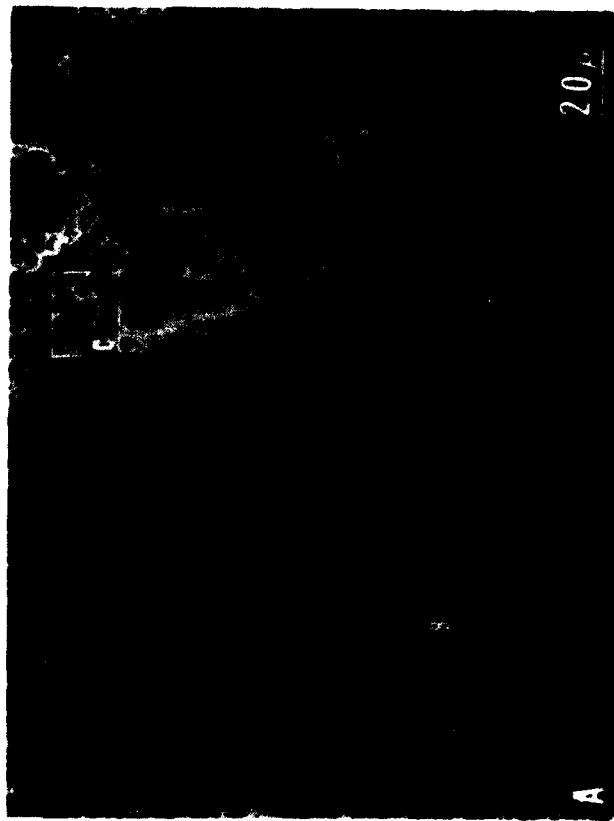


Figure 5. Scanning electron fractographs of a three point bend specimen broken after hydrogen charging.



(B) High magnification view of the quasi-cleavage fracture surface.



(C) High magnification of a region of ductile fracture.



Figure 6. Scanning electron micrograph of the quasicleavage fracture surface after three-step etching with the reagent proposed in ref. 12. The outlined etch pit has a shape indicating a fracture plane near  $\{110\}$



Figure 7. Scanning Electron micrograph of the fracture surface in the specimen embrittled by hydrogen. The specimen has been etched to reveal the lath structure.

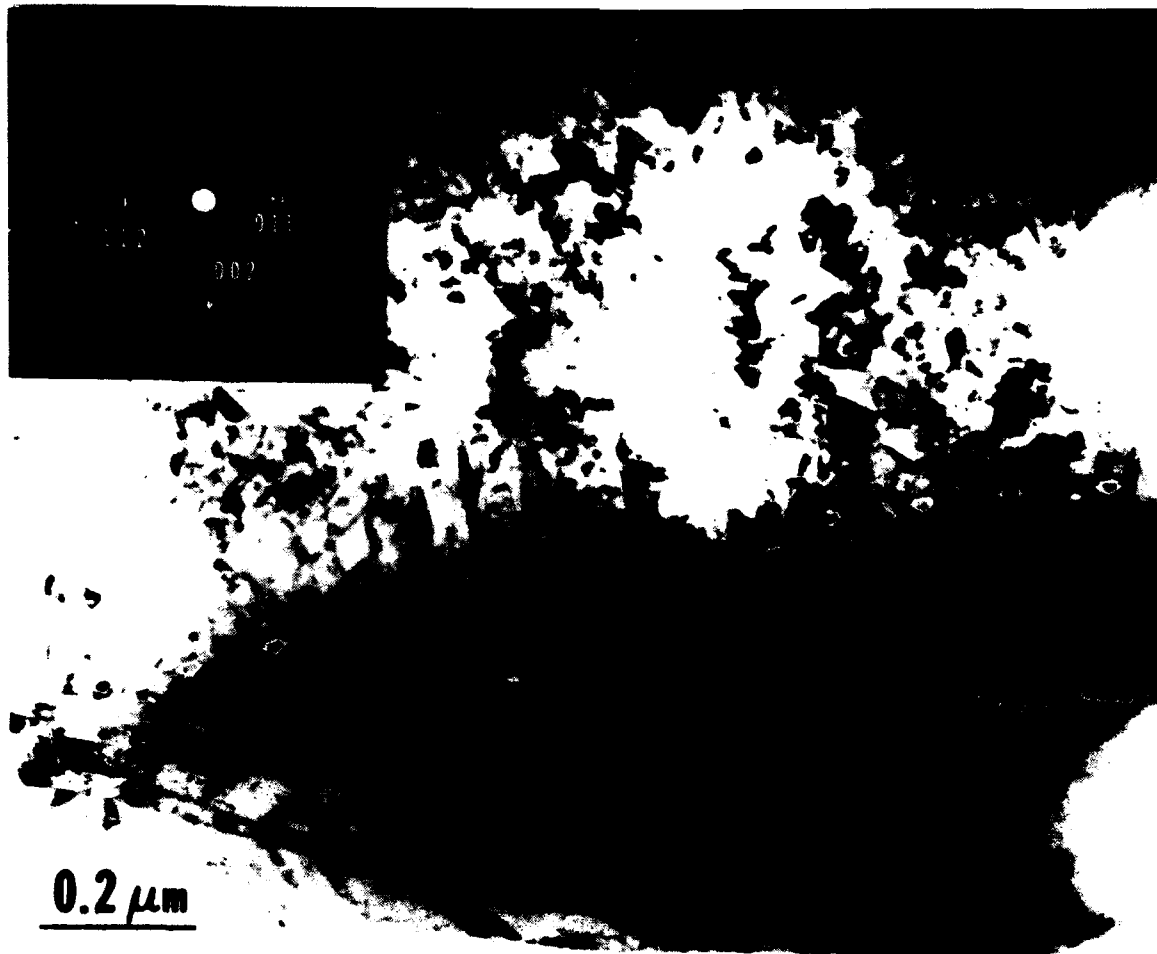


Figure 8. Transmission electron micrographs of the profile fractographic specimens showing the fracture surface and subsurface microcracks.

- (A) The fractograph shows the fracture surface (large arrows), a subsurface interlath crack (small arrow), and a subsurface diffraction pattern showing broadened diffraction spots that suggest plastic deformation.



Figure 8 (B) The fractograph shows the fracture surface (large arrows) and three subsurface interlath cracks (small arrows) which are nearly connected.

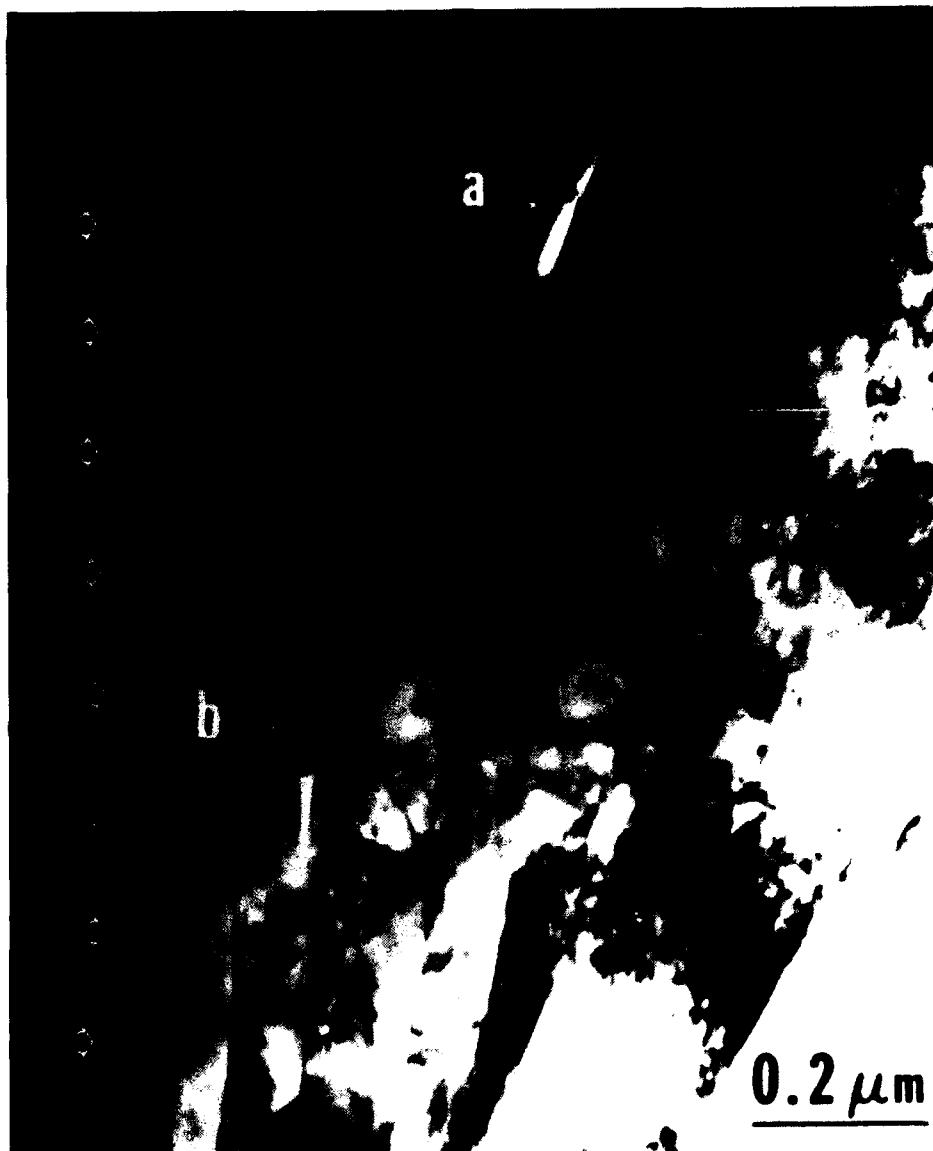


Figure 8 (C) The fractograph shows the fracture surface (large arrows), an interlath microcrack (a), and a microcrack within a lath (b) that apparently originates from a carbide particle.



Figure 8 (D) The fractograph shows the fracture surface (large arrows), apparent translath steps in the fracture surface (\*), the trace of the (110) plane, which is sensibly parallel to the fracture surface, and subsurface interlath microcracks (small arrows).

**END**

**FILMED**

**10-83**

**DTIC**